ADVANCED OPTICAL MATERIALS

Supporting Information

for *Adv. Optical Mater.*, DOI: 10.1002/adom.202000489

Nanoscale Optical Display and Sensing Based on the Modification of Fano Lineshape

Jin Xiang, Jingdong Chen, Sheng Lan, and Andrey E. Miroshnichenko**

Supplementary Information

Jin Xiang,[1#] Jindong Chen,[1#] Sheng Lan[1*], and Andrey E. Miroshnichenko[2*]

[1]*Guangdong Provincial Key Laboratory of Nanophotonic Functional Materials and Devices, School of Information and Optoelectronic Science and Engineering, South China Normal University, Guangzhou 510006, China*

[2]*School of Engineering and Information Technology, University of New South Wales, Canberra, ACT, 2600, Australia*

[#]Authors contribute equally to this work.

*Corresponding author: slan@scnu.edu.cn and andrey.miroshnichenko@unsw.edu.au

Table of contents

1. Morphology of Si nanoparticles distributed on a thin Au film…..…….……2

2. Contribution of gap modes to the total scattering……..2

3. Electric field enhancements without and with SPP excitation……...…….3

4. Scattering spectra of PS nanoparticles used to extract the spectra of SPPs……..…….4

5. SPPs generated on the surface of the Au film……..……..….…….5

6. Dependence of the scattering spectrum on the incidence angle……..…….....6

7. Fitting of the scattering spectra with Fano formula……..……...8

8. Mirror-image-induced magnetic dipole……..……...9

9. Dependence of the SPP wavelength on the incidence angle……...10

10. Dependence of the SPP wavelength on the environment refractive index.……....11

11. Dependence of the scattering spectrum on the polarization of the incident light..12

12. Si nanoparticle placed on a thin Ag film……..……13

1. Morphology of Si nanoparticles distributed on a thin Au film

Supplementary Fig. 1 shows the scanning electron microscopy image of Si nanoparticles with different diameters fabricated by using femtosecond (fs) laser ablation in water. They were randomly distributed on a Au/SiO_2 substrate with a 50-nm-thick Au film.

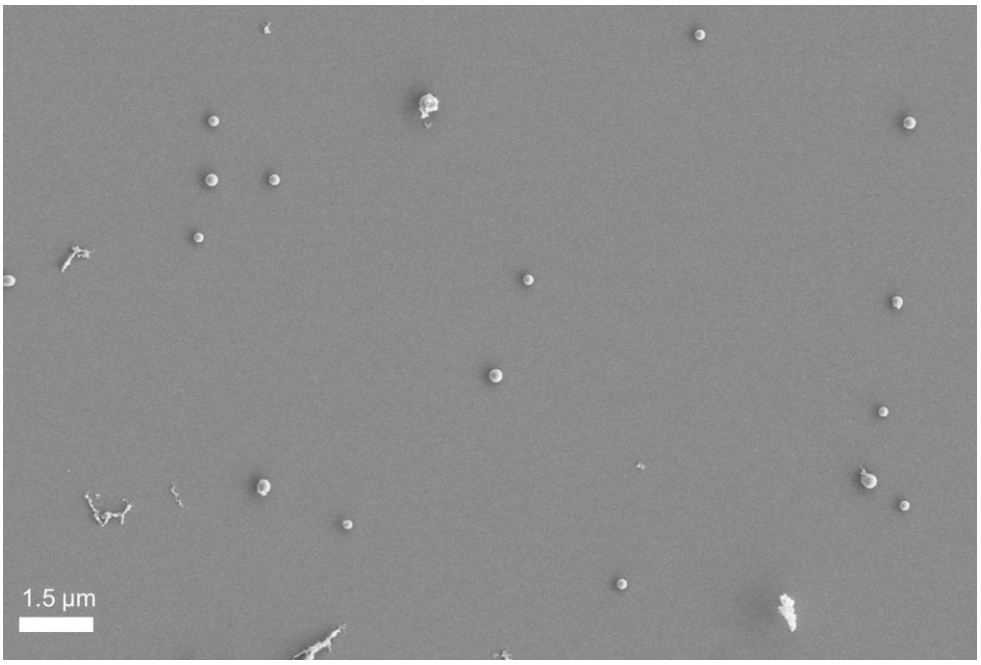

Supplementary Fig. 1 | Scanning electron microscopy image of Si nanoparticles randomly distributed on a Au/SiO_2 substrate.

2. Contribution of gap modes to the total scattering

For a Si nanoparticle placed on a thin Au film, gap modes oriented in the *x* and *z* directions, which are denoted as g_x and g_z, are expected to exist in the gap region between the Si nanoparticle and the Au film. Basically, g_x and g_z are excited by horizontally and vertically oriented electric field (E_x and E_z) of the SPPs and radiate in the *z* and *x* directions, respectively. Therefore, the contribution of g_z to the scattering detected in the *z* direction can be neglected. In order to examine the contribution of gap modes to the total scattering, we calculated the scattering spectra of a Si nanoparticle with different gap widths, as shown in Supplementary Fig. 2a. With increasing gap width, a small redshift of the Fano dip is observed, leading to the small change of the spectral shape (or Fano lineshape). This behavior

indicates that the subradiant mode originates from the coherent interaction of electric dipole p_x and its mirror image (p_{xm}), whose resonant wavelength is determined by the separation between p_x and p_{xm}. For a large gap width (e.g., g > 10 nm), the gap mode g_x disappears completely, as confirmed by the calculated charge distrinutions shown in Supplementary Fig. 2b. In this case, only very weak gap mode g_z is left and its contribution to the total scattering is negligible. Apart from the small change in the spectral shape (i.e., Fano lineshape), the scattering intensity does not change so much when the gap width is increased to g = 20 nm, implying that the superradiant mode involved in the formation of the Fano dip originates from the coherent interaction of magnetic dipole and its mirror images (i.e., m_y and m_{ym}), as we discussed in the main text.

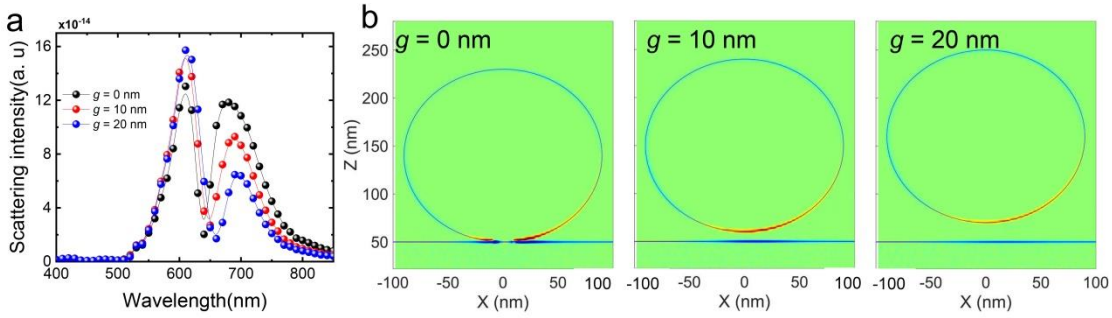

Supplementary Fig. 2 | a, Scattering spectra calculated for a Si NS with d ~ 180 nm which is separated from the Au film by different distances of g = 0, 10 and 20 nm. The calculated charge distributions for different gap widths are shown in **b**.

3. Electric field enhanments without and with SPP excitation

When the incidence angle is smaller than the critical angle, no surface plasmon polaritons (SPPs) are excited and the electric and magnetic fields of the incident light decay rapidly after passing through the Au film, as shown in Supplementary Fig. 3. In this case, Si nanoparticles will be excited by the transmitted wave on the surface of the Au film. In sharp contrast, the electric and magnetic fields on the surface of the Au film are significantly enhanced when the SPPs are excited, as shown in Supplementary Fig. 3. As a result, Si nanoparticles can be

effective excited by the electromagnetic fields of the SPPs, leading to strong scattering SPPs into far-field light and the generation of Fano resonance in the forward scattering spectra.

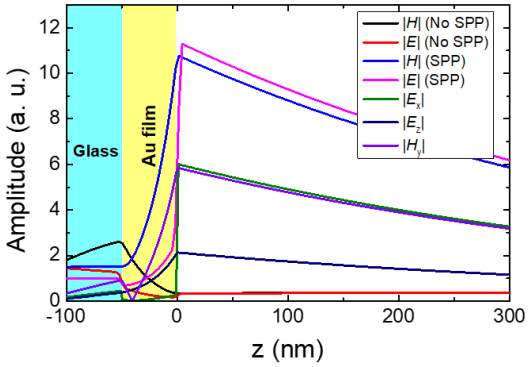

Supplementary Fig. 3 | Electric |*E*|, magnetic |*H*| field distributions and their components when the Au film is excited by a plane wave at incidence angles of 0° and 45°. The electric and magnetic fields are normalized to the incident field.

4. Scattering spectra of PS nanoparticles used to extract the spectra of SPPs

Basically, the spectra of the SPPs generated on the surface of the Au film at different incidence angles can be extracted from either the spectra of the reflected light or the spectra of a nanoparticle without any resonance in the visible to near infrared spectral range. In our experiments, we chose a polystyrene (PS) nanosphere with a diameter of 200 nm as the scatter for the SPPs. The calculated scattering spectrum of the PS nanosphere in free space is shown in the Supplementary Fig. 4. It can be seen that no resonance is found in the scattering spectrum, implying that the scattering spectra of the SPPs can be extracted from those of the PS nanosphere excited by the SPPs, as shown in Fig. 3c,d.

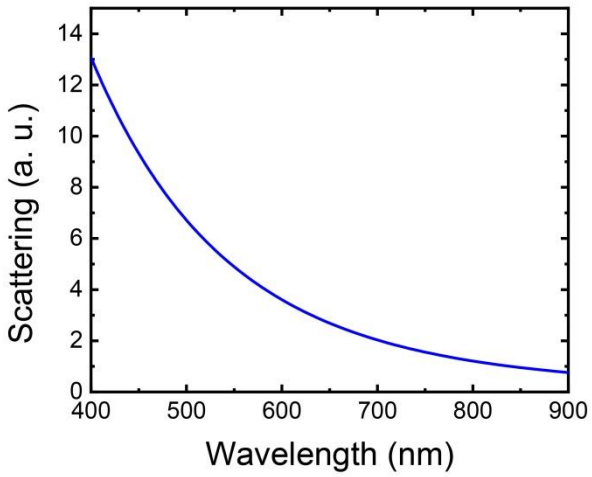

Supplementary Fig. 4 | Scattering spectrum calculated for a PS NS with d = 200 nm in free space.

5. SPPs generated on the surface of the Au film

The Si nanospheres (NSs) placed on the Au film (see Supplementary Fig. 1) can be excited either by the evanescent wave or the SPPs generated on the surface of the Au film, depending on the incidence angle of the excitation light. In the first case, the angle of the incident light (~33°) was smaller than the critical angle for total internal reflection (~43°) and no SPPs were excited on the surface of the Au film. As a result, only the mirror-image-induced magnetic dipole, which appeared as a sharp resonant mode, was observed in the scattering spectra, as shown in the left panel of Supplementary Fig. 5. In comparison, one can observe distinct Fano resonances embedded in the broad scattering spectra when the incidence angle exceeds the critical angle. In particular, the intensities of the two scattering peaks are almost equal when the incidence angle is appropriately chosen, as shown in the right panel of Supplementary Fig. 5. In both cases, vivid scattering light can be observed, as shown in the insets of Supplementary Fig. 5.

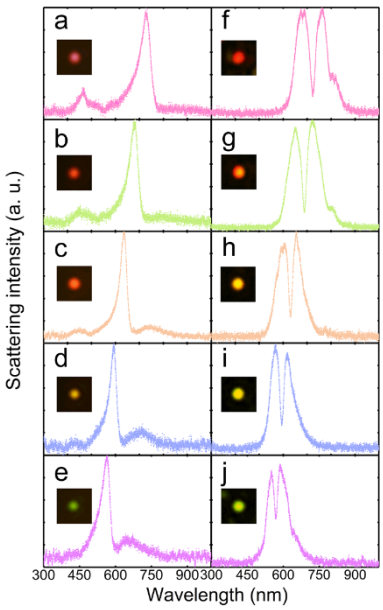

Supplementary Fig. 5 | Scattering spectra measured for Si NSs with different diameters without (left panel, **a**-**e**) and with (right panel, **f**-**j**) SPP excitation. The CCD images of the scattering light are shown in the insets.

6. Dependence of the scattering spectrum on the incidence angle

In Supplementary Fig. 6, we show the evolution of the scattering spectrum with decreasing incidence angle from 49° to 39° measured for a Si NS with d ~ 190 nm. From the image recorded by using a charge coupled device (the one enclosed with a dashed circle), one can clearly see the change of the scattering light from green to red when the incidence angle was reduced from 50° to 45.5° (see Supplementary Fig. 7). Under a dark-field microscope, the scattering light of the Si NS appeared as red.

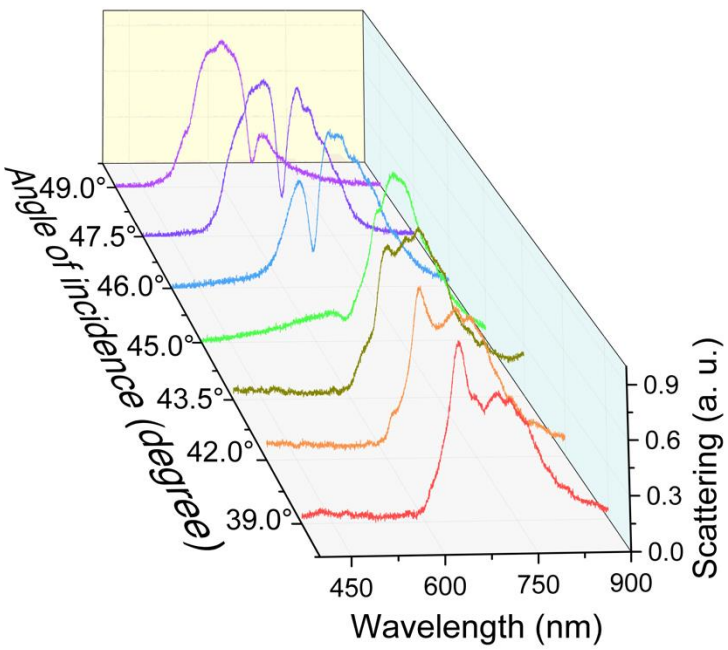

Supplementary Fig. 6 | Evolution of the scattering light of the Si NS with d ~ 190 nm with decreasing incidence angle.

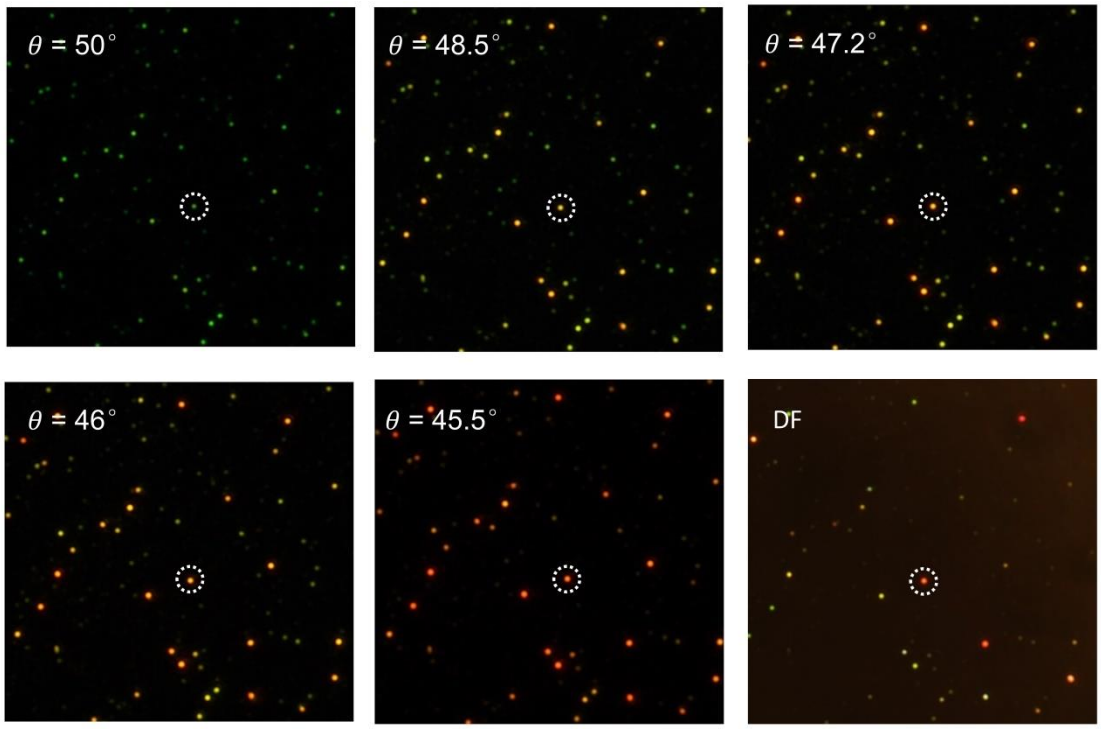

Supplementary Fig. 7 | Evolution of the scattering light of a Si NS with d ~ 190 nm with decreasing incidence angle. The dark-field microscope image of the Si NS (DF) is also provided for comparison.

7. Fitting of the scattering spectra with Fano formula

As described in detail in the Methods section, the scattering spectra of the Si NSs can be well fitted by using the formula of Fano resonance. In each case, the parameters involved in the formula (i.e., ω_s, W_s, ω_a, W_a, a, b, q) can be extracted. In Fig. 2, the static manipulation of the q parameter is achieved by changing the size of the Si NS. The parameters used for the fitting of the scattering spectra are provided in Table I. In this case, the values of ω_s, W_s, and W_a remain nearly unchanged when the size of the Si NS is varied. Only the value of ω_a is changed with the size of the Si NS, implying the modification of the resonant frequency of the subradiant mode. In Fig. 5a, the dynamical manipulation of the q parameter is realized by varying the incidence angle and the parameters used for the fitting of the scattering spectra are listed in Table II. It can be seen that the values ω_a and W_a do not change so much when the incidence angle is changed. In comparison, the values of ω_s and W_s are varied with decreasing the incidence angle, indicating the shift of the SPP wavelength with the incidence angle. As shown in Fig. 5c, the Fano lineshape is quite sensitive to the slight change in the environment refractive index and it is reflected clearly in the change of the q value. The parameters used for fitting the scattering spectra of the Si NS with d = 188 nm shown in Fig. 5c are listed in Table III.

Table I: Parameters used for fitting the scattering spectra measured for Si NSs with different diameters which are shown in Fig. 2.

Si NS	a	ω_s	W_s	ω_a	W_a	q	b
a	1.10	1.97	0.20	1.83	0.03	-0.30	0.20
b	1.05	1.97	0.20	1.86	0.03	-0.15	0.20
c	1.15	1.98	0.20	1.97	0.04	-0.03	0.15
d	1.05	1.99	0.20	2.23	0.03	0.30	0.45
e	1.05	1.99	0.20	2.17	0.03	0.47	0.52

Table II: Parameters used for fitting the scattering spectra measured for the Si NS with d ~ 188 nm at different incidence angles which are shown in Fig. 5a.

	a	ω_s	W_s	ω_a	W_a	q	b

θ= 50.0 °	1.05	2.37	0.15	2.22	0.04	-0.18	0.25
θ = 48.5°	1.10	2.30	0.17	2.23	0.04	-0.1	0.17
θ = 47.2°	1.37	2.23	0.14	2.23	0.04	0	0.1
θ = 46.5°	1.10	2.14	0.17	2.245	0.04	0.2	0.17
θ = 46.0°	1.10	2.05	0.17	2.25	0.035	0.4	0.10

Table III: Parameters used for fitting the scattering spectra calculated for the Si NS with d = 188 nm embedded in environments with different refractive indices which are shown in Fig. 5c.

	a	ω_s	W_s	ω_a	W_a	q	b
n = 1.00	2.2	2.00	0.09	1.93	0.21	-0.5	0.05
n = 1.02	3.0	2.01	0.09	1.99	0.21	-0.12	0.03
n = 1.025	3.2	2.01	0.09	2.01	0.21	0	0.03
n = 1.03	3.1	1.98	0.09	2.07	0.21	0.35	0.04
n = 1.04	2.8	2.00	0.1	2.14	0.21	0.55	0.03

8. Mirror-image-induced magnetic dipole

The Au film plays an important rople in determining the scattering properties of the Si nanoparticle. Based on the mirror image theory, the scattering spectrum of the Si nanoparticle is determined by the coherent interactions of the ED and MD excited in the Si nanoparticle with their mirror images induced by the Au film. In Supplementary Fig. 8a, we compared the scattering spectra and field distributions of a Si nanoparticle (d = 190 nm) for two incidence angles (θ) of 0° and 45.3°, which are smaller and larger than the critical one (~43°). For θ = 0°, the scattering spectrum is dominated by the radiation of the mirror-image-induced magnetic dipole whose resonant wavelength appears at ~645 nm. In shape contast, a pronounced Fano dip is ceated exactly at ~645 nm for θ = 45.3° when the SPPs are excited. This phenomenon indicates that the subradiant mode involved in the formation of the Fano resonance is the mirror-image-induced MD, which originates from the ED and its mirror image. In Supplementary Fig. 8b, we show the electric field distribution calculated for the Si nanoparticle on the Au film for θ = 0°. The electric

field distribution calculated for a Si nanoparticle dimer is provided in Supplementary Fig. 8d for comparison. It is remarkable that the electric field distrinution of the Si nanoparticle on the Au film is almost the same as that in the upper Si nanoparticle in the Si nanoparticle dimer. This behavior indicates clearly that the mirror image theory can be employed to describe the scattering behavior of the Si nanoparticle on the metal film.

In order to confirm the formation of the mirror-image-induced MD for the Si nanoparticle excited by the SPPs, we also calculated the magnetic field distribution on the xy plane (i.e., on the surface of the Au film), as shown in Supplementary Fig. 8c. It is noticed that the maximum magnetic field is achieved at the contacting point between the Si nanoparticle and the Au film. More importantly, the orientation of the magnetic field at this position is along the y direction, which confirms undoubtly the formation of the mirror-image-induced MD.

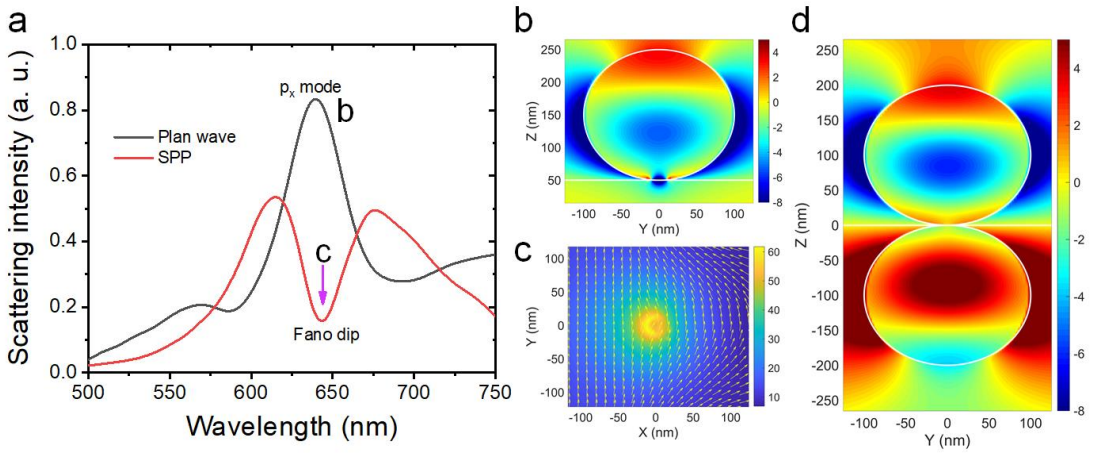

Supplementary Fig. 8 | a, Scattering spectra of a Si nanoparticle (d = 190 nm) excited by a plane wave and the SPPs, respectively. The incidence angles are chosen to be θ = 0° and 45.3°. **b**, Electric field distribution on the yz plane calculated for the Si nanoparticle excited by a plane wave (θ = 0°). **c**, Magnetic field distribution on the xy plane calculated for the Si nanoparticle excited by the SPPs (θ = 45.3°). **d**, Electric field distribution on the yz plane calculated for a Si nanoparticle dimer excited by a plane wave (θ = 0°).

9. Dependence of the SPP wavelength on the incidence angle

The relationship between the SPP wavelength and the incidence angle can be described as follows:

$$k_{sppx} = k_{px},$$

where $k_{sppx} = \frac{\omega}{c}\sqrt{\frac{\varepsilon_m \varepsilon_n}{\varepsilon_m + \varepsilon_n}}$, $k_{px} = \frac{\omega}{c}\sqrt{\varepsilon_p}\sin\theta$

Based on the complex refractive index of gold, the relationship between the SPP wavelength and the incidence angle can be extracted, as shown in Supplementary Fig. 9a. It can be seen that the SPP wavelength is redshifted with decreasing incidence angle and it becomes quite sensitive to the incidence angle near the critical angle. The phase change at a cerian wavelength induced by the shift of the SPP wavelength with the incidence angle can be seen in Supplementary Fig. 9b.

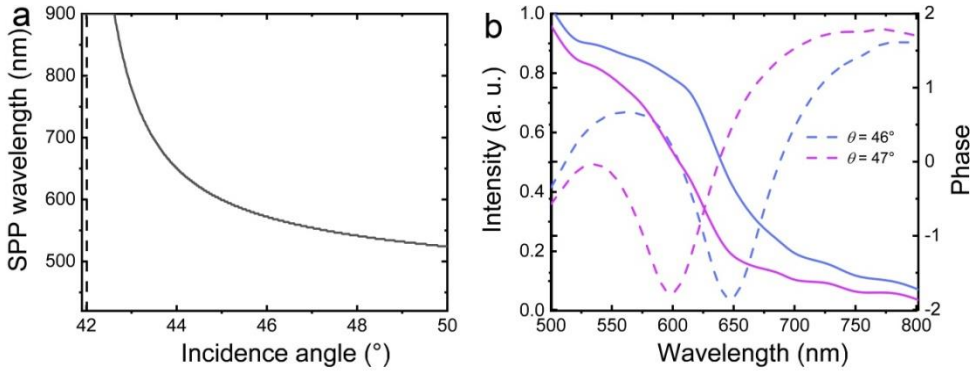

Supplementary Fig. 9 | a, Dependence of the SPP wavelength on the incidence angle. **b**, Phase spectra calculated for SPPs generated at different incidence angles.

10. Dependence of the SPP wavelength on the environment refractive index

Apart from the incidence angle, the SPP wavelength is also very sensitive to the refractive index of the environment, which is assumed to be air in our case. In Supplementary Fig. 10a, we present the dependence of the SPP wavelength on the environment refractive index calculated at different incidence angles. It is remarkable that the SPP wavelength becomes extremely sensitive to the environment refractive index when the incidence angle approaches the critical one. As a result, the Fano line shape will become more sensitive to the change of the environment refractive index, as shown in Supplementary Fig. 10b. In this case, however, the SPP wavelength is redshifted from visible light to near infrared spectral range when the incidence angle approaches the critical one and the variation of the Fano line shape is not directly reflected in the change of the scattering light color.

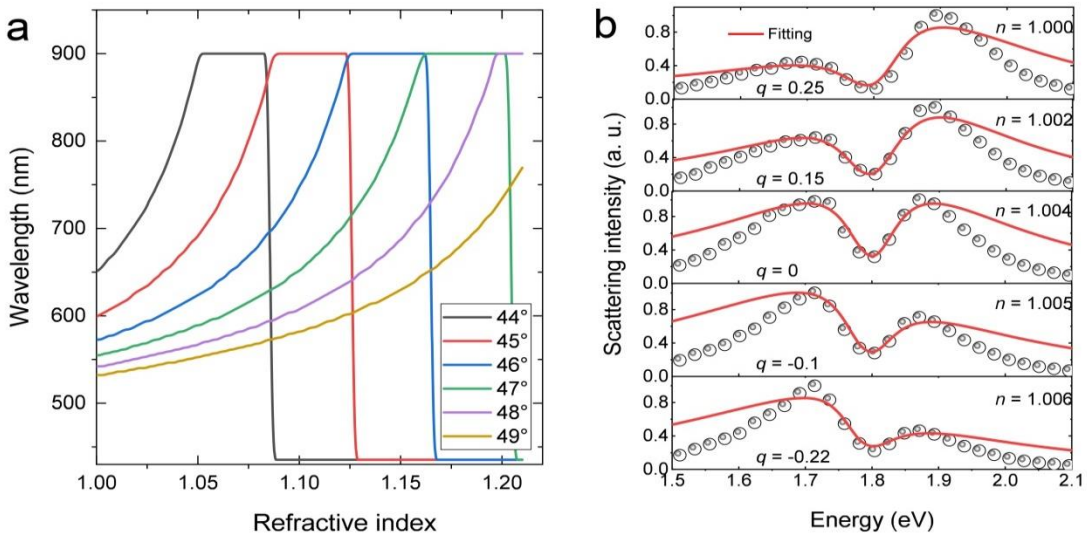

Supplementary Fig. 10 | a, Dependence of the SPP wavelength on the environment refractive index calculated at different incidence angles. **b**, Evolution of the Fano line shape with increasing environment refractive index calculated at an incidence angle of 46.5°.

11. Dependence of the scattering spectrum on the polarization of the incident light

In Supplementary Fig. 11, we show the scattering spectra calculated for the Si NS with d = 180 nm excited by using p- and s-polarized light with θ = 46.5°. For the s-polarized light, only a sharp resonant mode is excited. A Fano resonance, which is close to the sharp resonant mode, is formed in the scattering spectrum when the p-polarized light is employed. Significantly enhanced scattering light originating from the SPP excitation of the Si NS is observed. It means that one can readily manipulate the scattering spectrum of the hybrid system by simply changing the polarization of the incident light.

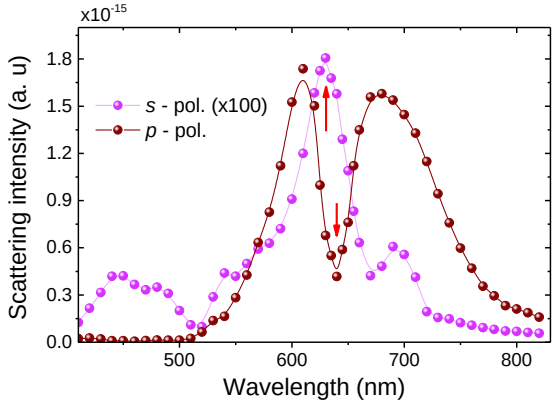

Supplementary Fig. 11 | Scattering spectrum calculated for a Si NS with d ~ 180 nm excited by using p- and s-polarized light at θ = 46.5°.

12. Si nanoparticle placed on a thin Ag film

We also examined the Fano resonance formed in the scattering spectrum of a Si nanoparticle placed on a thin silver (Ag) film, which possesses a smaller Ohmic loss in the visible light spectrum, and excited by the SPPs generated on the surface of the Ag film. In Supplementary Fig. 12a, we show the dependence of the Fano lineshape on the incicence angle at which the SPPs are generated. It can be seen that the reversal of the asymmetric parameter q can be realized by slightly chaning the incidence ange from 45.2° to 45.3°, implying a higher sensitivity of the Fano lineshape to the incidence angle as compared with the Si nanoparticle on the Au film. In Supplementary Fig. 12b, we present the electric field calculated on the yz plane. It is found that a larger enhancememnt factor for the electric field (~170) is achieved at the contacting point between the Si nanoparticle and the Ag film, which is more useful for realizing strong light-matter interaction.

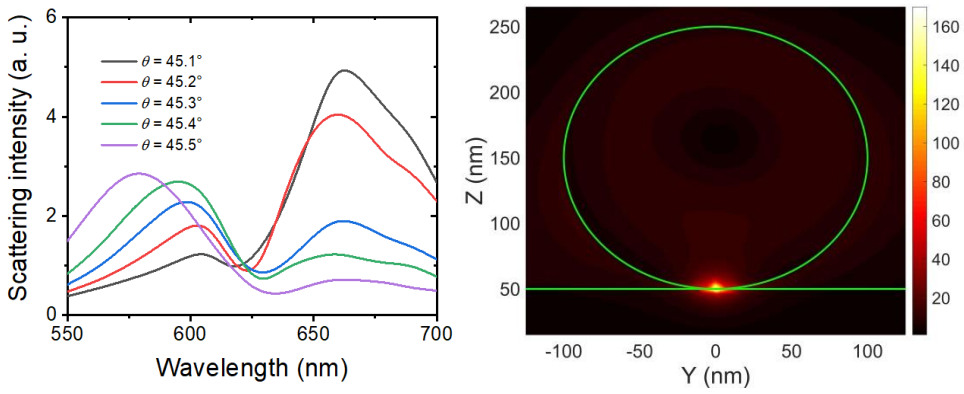

Supplementary Fig. 12 | a, Dependence of the Fano lineshape on the incidence angle calculated for a Si nanoparticle (d = 200 nm) placed on a thin Ag film. **b**, Electric field distribution calculated on the yz plane for the Si nanoparticle (d = 200 nm) placed on a thin Ag film.